Contents lists available at SciVerse ScienceDirect

CIRP Annals Manufacturing Technology

Journal homepage: www.elsevier.com/locate/cirp

Microstructure Based Flow Stress Model to Predict Machinability in Ferrite-Pearlite Steels

M. Saez-de-Buruaga[a], P. Aristimuño[a], D. Soler[a], E. D'Eramo[b], A. Roth[b], P.J. Arrazola (1)[a]

[a]*Faculty of Engineering, Mondragon University, Mondragon 20500, Spain*
[b]*Ascometal-Creas, Hagondange 57301, France*

A new flow stress model is proposed to describe the behaviour of ferrite-pearlite steels based on microstructure properties, including the effect of high strains, strain rates and temperatures. The model introduces strain hardening as a function of the pearlite ratio, interlamellar spacing and ferrite grain size. A non-linear thermal softening, and the coupling between strain rate and temperature are also introduced. Tested on a 2D ALE model, predicted cutting forces, tool temperatures, chip thickness and tool wear results obtained good agreement when compared to orthogonal cutting tests of four ferrite-pearlite steels, covering a wide range of microstructure variants.

Modelling, Micro structure, Flow Stress

1. Introduction

In the course of studying the influence of workpiece materials on cutting performance, most numerical research is focused on the calculation of fundamental machining variables (cutting forces, temperatures, strains, strain rates, tool stresses, etc.) during the chip forming process. Obtaining variables of industrial relevance (wear, surface integrity) is more complex, and in general the results obtained to date are not as effective as industry requires [1]. The reasons for this are several: difficulties in obtaining correctly identified input parameters, very simple material and contact behaviour models that do not reflect the real process, very high calculation times in 3D models, etc. As a consequence, numerical modelling is still a developing technique, where inputs such as friction and material flow stress laws are of great influence in obtaining precise fundamental physical as well as relevant industrial results [2].

In this context, most of the material flow stress laws applied in the codes are based on phenomenological models, where the JC model [3] and variations of this [4] prevail as the most widely used. Recently developed models in which the strain rate is considered to be coupled with temperature [5], have demonstrated greater degree of accuracy for the case of cutting nickel based alloys.

Physically based models (microstructure or phase level) are still a challenge today. As an example, in the case of ferrite-pearlite steels, it enables the modelling of the individual behaviour of ferrite and pearlite, which involves an advance in material forming processes [6]. However, their development for the extreme thermomechanical conditions occurred in machining is still not validated.

2. Scientific framework

This research focuses on the development and validation of a procedure to model the chip formation process, capable of predicting the influence that the microstructure of the material has on machinability/tool wear. The analysis is focused on the study of carbon steels, where the microstructure type is that of Ferrite - Pearlite (FP). These are materials widely used in the automotive industry, in which processing by machining is a common operation. To achieve the objective, the required inputs are identified as dependant on the microstructure, in which the greatest effort has been focused on the development of a flow stress model based on microstructure. Considering the limitations of the current constitutive models, this should represent the following aspects:

- Material behaviour under high strain, strain rates and temperatures, and even the coupled effects between these abovementioned phenomena.
- Distinguish the behaviour of FP steels based on microstructure input.

As a case study, four FP steels are selected to cover a wide range of microstructure variants: 16MnCr5 (16), 27MnCr5 (27), C45 (45) and C60 (60) steels. Their main microstructure characteristics are summarized in Table 1, and compositions in Table 2.

Table 1
Quantitative analysis of ferrite-pearlite ratio (%), ferritic and pearlitic grain size (μm) and interlamellar spacing (nm) [7]

	16MnCr5	27MnCr5	C45	C60
%ferrite/%pearlite	58 / 42	40 / 60	25 / 75	14 / 86
Grain size ferrite	10	14	17	11
Grain size pearlite	13-15	15	22-27	31
Interlamellar spacing	190±65	285±75	293±82	372±135

Table 2
Chemical composition of steel grades (%) [7]

	C	Mn	Si	Cu	Ni	Mo	Al
16MnCr5	0.19	1.23	0.17	0.17	0.19	0.07	0.020
27MnCr5	0.25	1.19	0.24	0.11	0.09	0.04	0.032
C45	0.45	0.78	0.33	0.11	0.09	0.02	0.007
C60	0.61	0.65	0.28	0.24	0.14	0.04	0.005

3. MicroStructure Based flow stress model proposal

The MicroStructure Based (MSB) flow stress model is proposed as Eq. 1. Strain hardening (σ_{SH}), thermal softening (σ_{TS}) and strain rate hardening (σ_{SRH}) terms are modelled separately. A particular feature is dependence of σ_{SRH} on both $\dot{\varepsilon}$ and T (σ_{SH} has units of stress, σ_{TS} and σ_{SRH} are both dimensionless).

$$\sigma = \sigma_{SH}(\varepsilon) \cdot \sigma_{TS}(T) \cdot \sigma_{SRH}(\dot{\varepsilon}, T) \quad (1)$$

Only σ_{SH} is obtained here from ferrite-pearlite content. σ_{TS} and σ_{SRH}, assumed alike for all the steels, are obtained by experiment.

3.1. Strain hardening (σ_{SH})

The strain hardening evolution was developed in [7] and is based on a rule of mixtures [6] for the macro-flow stress and macro-strain increment (Eq. 2), with α denoting ferrite and p pearlite, and f_p the volume fraction of pearlite. Strain is shared between ferrite and pearlite by an iso-work assumption (Eq. 3).

$$\sigma_{SH} = (1 - f_p)\sigma_\alpha(\varepsilon_\alpha) + f_p\sigma_p(\varepsilon_p) \quad (2)$$
$$d\varepsilon = (1 - f_p)d\varepsilon_\alpha + f_p d\varepsilon_p$$

$$\sigma_\alpha(\varepsilon_\alpha)d\varepsilon_\alpha = \sigma_p(\varepsilon_p)d\varepsilon_p \quad (3)$$

σ_α follows a dislocation forest-hardening model, Eq. 4, modified from [6]. σ_0^α is the ferrite lattice friction, X^α is its kinematical hardening, α_n is a constant related to forest hardening ($\alpha_n = 0.4$), M is the mean Taylor factor (M=3), μ_α is the ferrite shear modulus ($\mu_\alpha = 80$ GPa), b is the Burger's vector ($b = 2.5 \cdot 10^{-10}$m), and ρ^α is the statistically stored dislocation density.

$$\sigma_\alpha(\varepsilon_\alpha) = \sigma_0^\alpha + X^\alpha + \alpha_n M \mu_\alpha b\sqrt{\rho^\alpha} \quad (4)$$

Strain enters directly through X^α, Eq. 5, where d_α is the ferrite grain size. n_0 and λ_d are dimensionless, related to the critical density of geometrically necessary dislocations ($n_0 = 2.82$) and the density of shear bands ($\lambda_d = 34.5$) [6]. It also enters indirectly through dependence of ρ^α on strain, Eq. 6, from the balance between production and annihilation of dislocations [7]. f_{DRV} is an adjustable parameter related to the dynamic recovery ($f_{DRV} = 1.2$), k_0 latent hardening ($k_0 = 5.63 \cdot 10^{-3}$) and the other parameters are as for Eq. 5.

$$X^\alpha = \frac{M\mu_\alpha b}{d_\alpha}\left(n_0\left(1 - \exp\left(-\frac{\lambda_d \varepsilon_\alpha}{n_0}\right)\right)\right) \quad (5)$$

$$\frac{d\rho^\alpha}{d\varepsilon_\alpha} = M\left(\frac{\exp\left(-\frac{\lambda_d \varepsilon_\alpha}{n_0}\right)}{b \cdot d_\alpha} + \frac{k_0}{b}\sqrt{\rho^\alpha} - f_{DRV} \cdot \rho^\alpha\right) \quad (6)$$

σ_p has a more empirical description (Eq. 7), based on the strong assumption that only the ferrite between the cementite lamellae deforms plastically, where σ_0^p is the lattice friction of pearlite, s is the interlamellar spacing of pearlite, K and g are two empirical constants (K=38 GPa, g=61.7), and θ^{IV} is the stage IV hardening of pearlite (θ^{IV} = 100 MPa).

$$\sigma_p(\varepsilon_p) = \sigma_0^p + \frac{M\mu_\alpha b}{s} + \frac{K}{g}\left(1 - \exp\left(-\frac{g\varepsilon_p}{2}\right)\right) + \theta^{IV}\varepsilon_p \quad (7)$$

In [9], in line with the above strong assumption, σ_0^α and σ_0^p are taken to be identical ($\sigma_0^\alpha = \sigma_0^p = \sigma_0$), assuming the non-partition of substitutional elements between ferrite and austenite before pearlitic transformation. Within this framework, σ_0 depends on materials composition, taking into account the different solutes and interstitials in solid solution [6, 7]. The contribution that the elements in solution make to the lattice friction was initially suggested by [8]. Here the expression for σ_0 (Eq. 8) is adjusted better to reflect the influence of the solutes (concentrations are expressed in wt. %, σ_{00}=52 MPa, composition data in Table 2).

$$\sigma_0 = \sigma_{00} + 33Mn + 91Si + 8Cu + 4.5Ni + 8Mo + 4Al \quad (8)$$

σ_{SH} dependence on ε is built up from Eqs. 2-8, in increments of $d\varepsilon$, starting from $\varepsilon = 0$, and with material data from Tables 1, 2. Figure 1 shows the good agreement between the model results and experiments in uniaxial compression at 20°C and strain rate 0.5s^{-1}. The results of 16MnCr5 showed a constant deviation of 30 MPa above the experimental curves. This latter was linked to an extremely high pearlite banding and anisotropy found in the 16MnCr5, not accounted for in the model and which slightly altered the $\sigma_{SH}(\varepsilon)$ theoretical behaviour.

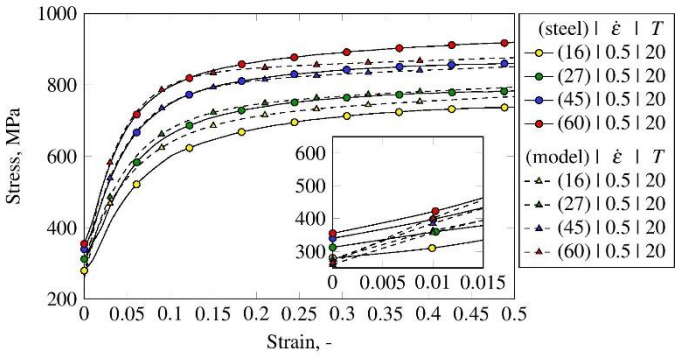

Figure 1. Comparison of predicted (dashed line) and experimental (solid line) flow stress curves at 20 °C and 0.5 s^{-1}

3.2. Thermal softening (σ_{TS})

Flow stress measured at temperature relative to flow stress at T_0 = 20°C is plotted against temperature in Figure 2. Results are fitted to the empirical Eq. 9, as in [5]. The steels have almost all the same softening, as initially assumed. m* = 0.0084°C^{-1} and B* = 914°C give a best fit.

$$\sigma_{TS}(T) = \frac{1}{1 + e^{m^*(T - B^*)}} \quad (9)$$

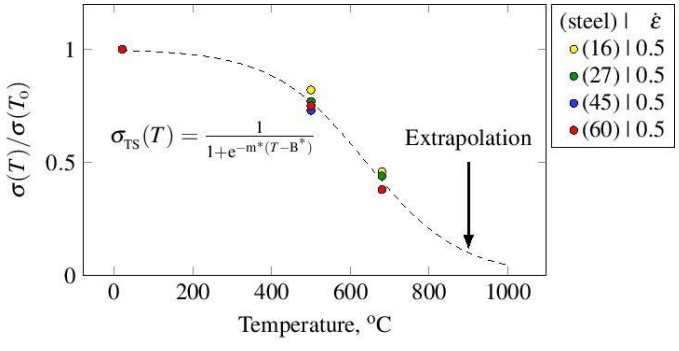

Figure 2. Characterization of the thermal softening term based on the flow stress at strain of 0.2 and strain rate of 0.5 s^{-1}

3.3. Strain rate hardening (σ_{SRH})

The influence of strain rate on flow stress has been determined from uniaxial compression tests at temperatures and strain rates up to 680°C and 4000s^{-1}. It is found that at constant temperature,

σ_{SRH} is not a true linear function of ln $\dot{\varepsilon}$ and further that it varies with temperature. It is found and proposed here that results may be fitted to a modified form, Eq. 10, of Johnson-Cook dependence [3] with the temperature dependence of C given by Eq. 11.

$$\sigma_{SRH}(\dot{\varepsilon}, T) = 1 + C(T) \cdot \left[\ln\left(\dot{\varepsilon}/\dot{\varepsilon}_0\right)\right]^{n^*} \quad (10)$$

$$C(T) = S^* + \frac{D^* - S^*}{1 + \left(\frac{T}{T_{sat}}\right)^r} \quad (11)$$

A best fit of results from all strain rates and temperatures, at a strain of 0.2, gives (Eq. 10) n* = 1.848 ($\dot{\varepsilon}_0$ = 0.5s^{-1}) and (Eq. 11) S* = 0.076, D* = 0.0064, r = 6.4 and T_{sat} = 1108K. Figure 3 compares experimental results at room temperature with the model prediction (the dashed line). Figure 4 plots experimental results in a way that compares experimental and model values of C(T). As with σ_{TS} all the steels have the same response. The extrapolated dependence of C(T) on T for T > 680°C counteracts thermal softening and is an important part of the model.

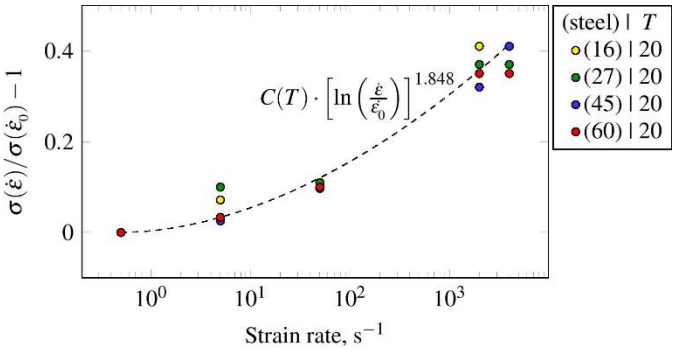

Figure 3. Characterization of the strain rate hardening exponent based on the yield stress at strain of 0.2 and temperature of 20°C

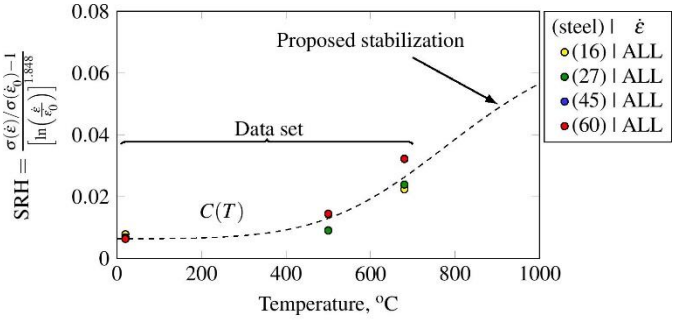

Figure 4. Characterization of the relationship between strain hardening term and temperature based on the yield stress at strain of 0.2

4. Evaluation of MSB flow stress model

Tool wear as well as tool forces and temperatures and chip thickness are predicted and compared with experimental results.

The MSB model is input to a FE orthogonal cutting model, with the Arbitrary Lagrangian Eulerian (ALE) approach, previously described in [9], selected as most suitable for executing the microstructure based inputs, for establishing a wear prediction strategy, and finally for predicting tool wear. One of the special characteristics of the developed FE model is a sliding velocity based friction law, developed first by [10] and fitted to FP steels depending on their ferrite fraction by [11]. Thermal properties were characterized for the selected steel and tool materials [7].

Tool wear prediction strategy is based on nodal displacement, with the same criteria as [12]. Basically, tool nodes are re-located depending on wear depth W, which is taken to increase with cut distance L, following [13]. $L = V_c \cdot \Delta t$, with V_c the cutting speed and Δt the cut time. Eq. 12 is the wear model, with a mechanical wear first term and a thermal wear second term. Tool wear tests show the steel has direct influence in the first term: $\frac{dW_{mechanical}}{dL}$ = 0.031 (%C) µm/m. For all the steels, A_w = 16257 µm/min and E_a = 87 kJ/mol [14] (V_c has units m/min.).

$$\frac{dW}{dL} = \frac{dW_{mechanical}}{dL} + \frac{A_w}{V_c} \cdot \exp\left[-\frac{E_a}{R \cdot T}\right] \quad (12)$$

Measurements of tool forces and temperatures, chip thickness, and rake and flank tool wear have been carried out in orthogonal conditions with all steels at feeds 0.1 and 0.2mm, speeds 100 and 200m/min, and depth of cut 2mm, with uncoated carbide tools (type P25, rake and clearance angles 5° and 6°). The temperature measurement details are published in [15].

4.1. Analysis of fundamental variables

Experimental and simulated chip thickness (t_2) are compared in Figure 5. Highly accurate agreements are seen except at V_c=200 m/min and f=0.2 mm when average differences are 12%. The decreasing t_2 with increasing pearlite is always predicted.

Cutting forces F_c are plotted in Figure 6. Predicted values slightly but systematically exceed experimental ones, with maximum differences of 20%.

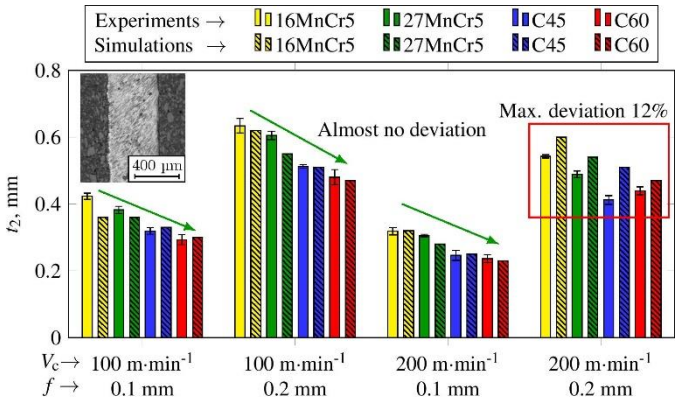

Figure 5. Experimental and simulation results of t_2 for all the FP steels and cutting conditions machined with fresh tools

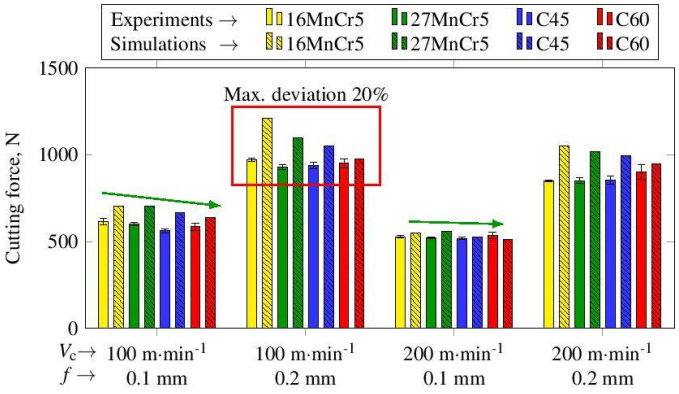

Figure 6. Experimental and simulation results of F_c for all the FP steels and cutting conditions machined with fresh tools

Tool temperature observations are summarised in Figure 7. Inset are shown simulated and experimentally obtained temperature fields for the case of a C45 steel (V_c = 200m/min and f = 0.2mm). Maximum tool temperatures from such views plotted in the main figure. Maximum differences between simulations and experiments are < 18%, while the average error is < 10%.

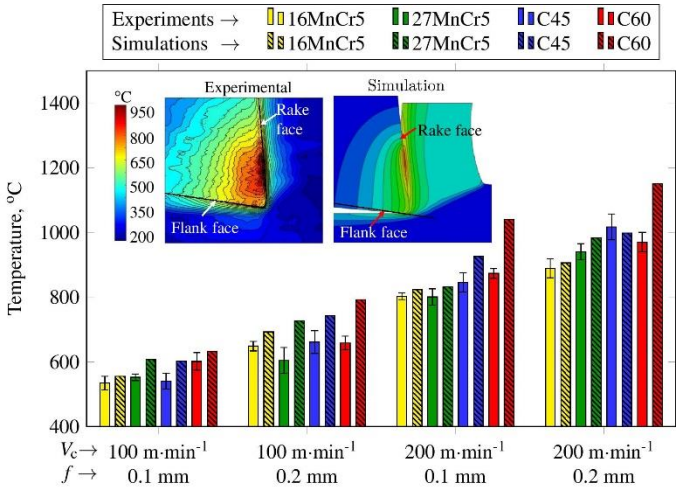

Figure 7. Experimental and simulation results of max. tool temperature machined with fresh tools and detail of thermal fields for a C45 steel

4.2. Analysis of machinability – tool wear

Figure 8 compares predicted and experimental crater depths K_T and flank wear lengths V_B after removing 480cm³ cut volume, with more detail of predicted crater and flank wear profile for each of the steels cut at V_c = 200m/min and f = 0.2mm.

The differences in both K_T and V_B between the steels are noticeable, with larger differences in K_T than V_B and C60 steel giving most wear in both cases. The predicted profiles show the changes in edge geometry as a result of wear.

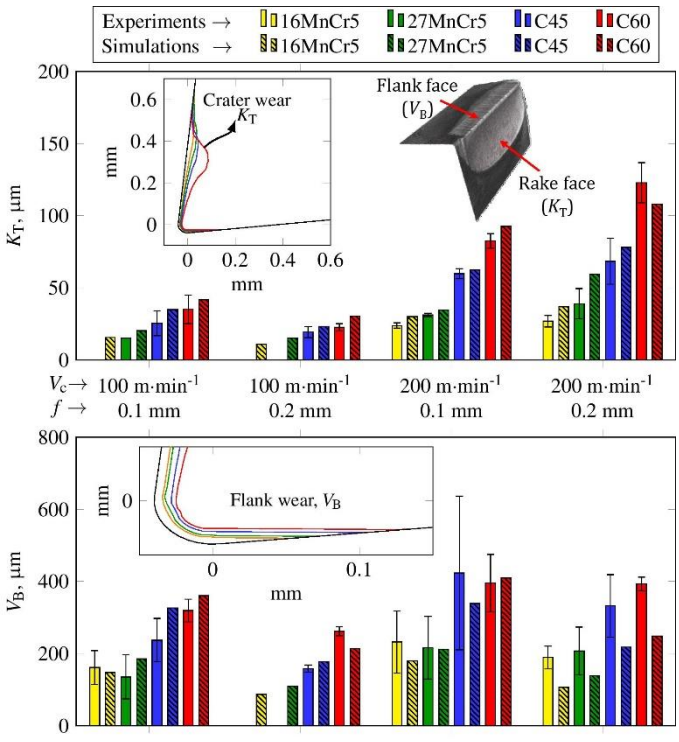

Figure 8. Experimental and simulation results of V_B and K_T after removing 480 cm³ cut volume, and detail of predicted worn profiles

In general, K_T is over-predicted, by up to 20%, though trend dependence on both steel type and cutting conditions is good. Predicted V_B are close to measured values, within measured deviations except for underestimates at V_c=200 m/min, f=0.2 mm. The overall deviation in the prediction of V_B is less than 20%. These levels of accuracy are believed to be of practical use.

5. Conclusions

The developed MSB model permits the qualitative prediction of machinability when integrated in an orthogonal cutting model and combined with a wear simulation strategy. In addition, the empirical procedure undertaken in this research permits the characterization of the wear rate law, and contributes to the data sets required for validation. In general, the trends observed in the simulations are in good agreement with the orthogonal cutting tests concerning both scientific and industrial relevant outputs. The values of crater depth (K_T) and flank wear land (V_B), and the scientific variables of cutting forces (F_c), chip thickness (t_2) and tool temperature are predicted with errors in the range 5-20%.

6. Acknowledgments

This work was supported by the projects IMMAC (RFSR-CT-2014-00020), MICROMAQUINTE (PI_2014_1_116) and EMULATE (DP12015-67667-C3-3R). The machining experimental tests and simulations were carried out at the University of Mondragon. The strain hardening term of the MSB model was developed within Ascometal-Creas. In addition we thank Prof. Tom Childs (Leeds University) for many helpful comments throughout the project.

References

[1] Arrazola, P. J., Özel, T., Umbrello, D., Davies, M., & Jawahir, I. S. (2013). Recent advances in modelling of metal machining processes. CIRP Annals, 62(2), 695-718.
[2] Melkote, S. N., Grzesik, W., Outeiro, J., Rech, J., Schulze, V., Attia, H., ... & Saldana, C. (2017). Advances in material and friction data for modelling of metal machining. CIRP Annals, 66(2), 731-754.
[3] Johnson, G. R. (1983). A constitutive model and data for materials subjected to large strains, high strain rates, and high temperatures. Proc. 7th Inf. Sympo. Ballistics, 541-547.
[4] Calamaz, M., Coupard, D., & Girot, F. (2008). A new material model for 2D numerical simulation of serrated chip formation when machining titanium alloy Ti–6Al–4V. International Journal of Machine Tools and Manufacture, 48(3-4), 275-288.
[5] Iturbe, A., Giraud, E., Hormaetxe, E., Garay, A., Germain, G., Ostolaza, K., & Arrazola, P. J. (2017). Mechanical characterization and modelling of Inconel 718 material behavior for machining process assessment. Materials Science and Engineering: A, 682, 441-453.
[6] Allain, S., & Bouaziz, O. (2008). Microstructure based modeling for the mechanical behavior of ferrite–pearlite steels suitable to capture isotropic and kinematic hardening. Materials Science and Engineering: A, 496(1-2), 329-336.
[7] Innovative method dedicated to the development of a ferrite-pearlite grade regarding its machinability - IMMAC (2018). RFSR-CT-2014-00020. Final report.
[8] Pickering, F. B., & Gladman, T. (1963). Metallurgical developments in carbon steels. ISI Special Report, 81(10).
[9] Arrazola, P. J., Arriola, I., Davies, M. A., Cooke, A. L., & Dutterer, B. S. (2008). The effect of machinability on thermal fields in orthogonal cutting of AISI 4140 steel. CIRP Annals-Manufacturing Technology, 57(1), 65-68.
[10] Zemzemi, F., Bensalem, W., Rech, J., Dogui, A., & Kapsa, P. (2008). New tribometer designed for the characterisation of the friction properties at the tool/chip/workpiece interfaces in machining. Tribotest, 14(1), 11-25.
[11] Arrieta, I., Courbon, C., Cabanettes, F., Arrazola, P. J., & Rech, J. (2017). Influence of the ferritic-pearlitic steel microstructure on surface roughness in broaching of automotive steels. In AIP Conference proceedings (Vol. 1896, No. 1, p. 090011).
[12] Klocke, F., & Frank, P. (2006). Simulation of tool wear in hard turning. In 9th CIRP International Workshop on Modelling of Machining Operations (pp. 11-12).
[13] Takeyama, H., & Murata, R. (1963). Basic investigation of tool wear. Journal of engineering for industry, 85(1), 33-37.
[14] Saez-de-Buruaga, M. (2018). A novel procedure based on 2D finite element modeling and orthogonal cutting tests to predict machinability and tool wear evolution considering the microstructure effect of lamellar ferrite-pearlite steels (Doctoral dissertation, University of Mondragon).
[15] Saez-de-Buruaga, M., Soler, D., Aristimuño, P. X., Esnaola, J. A., & Arrazola, P. J. (2018). Determining tool/chip temperatures from thermography measurements in metal cutting. Applied Thermal Engineering, 145, 305-314.